ACS NANO
Cite This: ACS Nano XXXX, XXX, XXX−XXX
www.acsnano.org

ARTICLE

Amyloid Fibrils Length Controls Shape and Structure of Nematic and Cholesteric Tactoids

Massimo Bagnani,[†] Gustav Nyström,[†] Cristiano De Michele,[‡] and Raffaele Mezzenga*[,†,§]

[†]Department of Health Science and Technology, ETH Zurich, Schmelzbergstrasse 9, LFO E23 Zurich 8092, Switzerland
[‡]Dipartimento di Fisica, "Sapienza" Università di Roma, P.le A. Moro 2, 00185 Roma, Italy
[§]Department of Materials, ETH Zurich, Wolfgang-Pauli-Strasse 10, Zurich 8093, Switzerland

Supporting Information

ABSTRACT: **Amyloid fibrils offer the possibility of controlling their contour length, aspect ratio, and length distribution, without affecting other structural parameters. Here we show that a fine control in the contour length distribution of β-lactoglobulin amyloid fibrils, achieved by mechanical shear stresses of different levels, translates into the organization of tactoids of different shapes and morphologies. While longer fibrils lead to highly elongated nematic tactoids in an isotropic continuous matrix, only sufficiently shortened amyloid fibrils lead to cholesteric droplets. The progressive decrease in amyloid fibrils length leads to a linear decrease of the anchoring strength and homogeneous tactoid → bipolar tactoid → cholesteric droplet transitions. Upon fibrils length increase, we first find experimentally and predict theoretically a decrease of the cholesteric pitch, before full disappearance of the cholesteric phase. The latter is understood to arise from the decrease of the energy barrier separating cholesteric and nematic phases over thermal energy for progressively longer, semiflexible fibrils.**

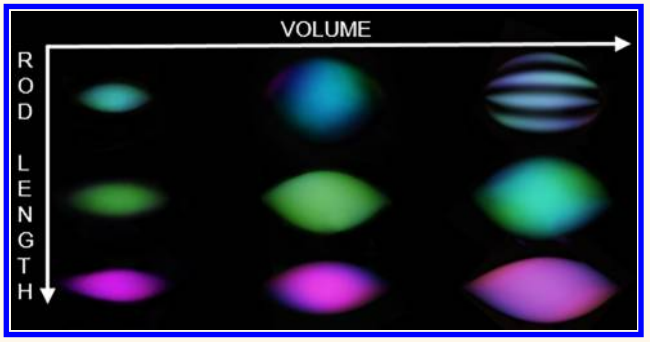

KEYWORDS: *chiral rods, liquid crystals, water-in-water emulsions, twist, chiral nematic, Frank−Oseen*

The spontaneous liquid crystalline phase transitions of particle suspensions have been deeply investigated both theoretically and experimentally on a wide class of rod-like colloids, from minerals to biological compounds.[1−4] Depending on the properties of the particles and on the environmental conditions, the anisotropic phase can be of various levels of order, such as nematic, smectic, columnar, discotic, *etc.* For particles possessing a chiral nature, the simplest form of liquid crystal order, the nematic phase, can be characterized by a wave function describing the orientation of the director along which the particles are principally oriented; such a phase is referred to as the chiral nematic or cholesteric liquid crystalline phase.[5] The cholesteric phase displays, on average, a helical arrangement of the orientation of the anisotropic particles, with the director field parametrized by a relationship of the type $n(z)=\{\cos(2\pi/p)z,\ \sin(2\pi/p)z,\ 0\}$, where z is the coordinate position on the cholesteric axis for a uniaxial orientation and p is the cholesteric pitch that determines the length scale associated with a complete twist of the helical periodicity. This helical organization characterizes many structural elements in natural systems[3] such as bones (collagen),[6] arthropods exoskeleton (chitin),[7] or plants (cellulose)[8] and is of particular interest in physics and technology, since some of their inherent properties can be exploited into advanced photonic applications, ranging from security papers to tunable mirrorless lasers.[9−13] As stated above, in general, the condition for the establishment of a chiral nematic phases is the chiral nature of the rod-like particle. However, fibrillar chirality alone does not guarantee the existence of a chiral nematic order, that is, the condition is necessary but not sufficient, and the fundamental connection between chirality at the single particle level up to the chiral liquid crystalline phases remains a highly debated problem.[14−17]

Amyloid fibrils are protein-based anisotropic colloids formed through self-assembly of β-sheet aggregates into twisted or helical ribbons. Initially discovered *in vivo* in the context of some devastating neurodegenerative disorders, including Alzheimer's and Parkinson's diseases, they have recently attracted increasing attention in biofunctional materials such as aerogels, catalytic scaffolds, bioavailable iron delivery, and functional coatings.[18−21] These fibrils are known to form nematic liquid crystal phases,[22−26] and although amyloid fibrils are chiral in nature, for a long time the nematic phase has

Received: October 3, 2018
Accepted: December 13, 2018
Published: December 13, 2018

DOI: 10.1021/acsnano.8b07557
ACS Nano XXXX, XXX, XXX−XXX

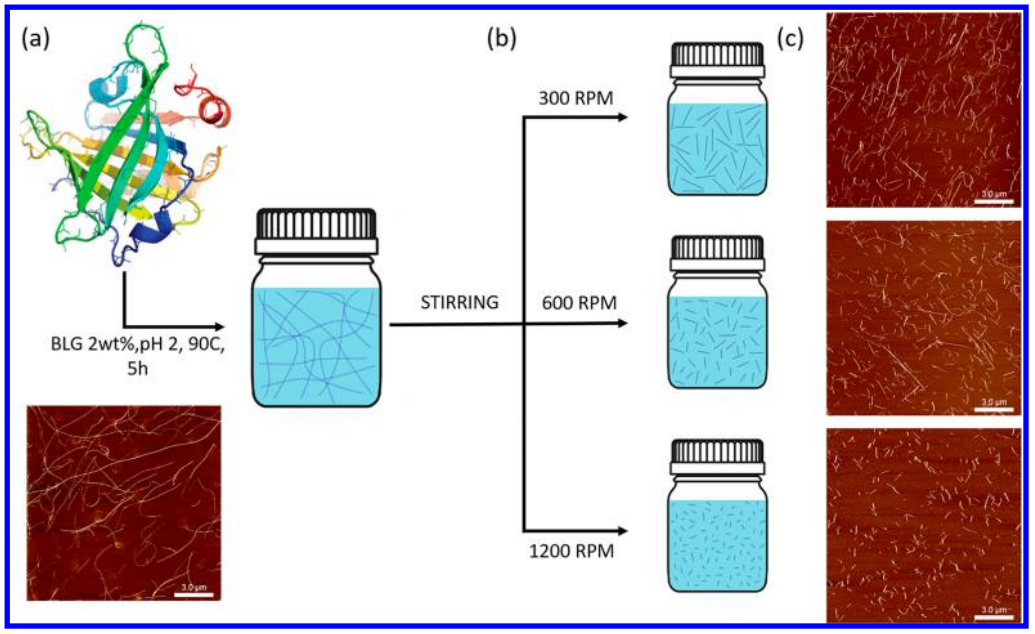

Figure 1. Preparation of amyloid fibrils with different aspect ratios studied in this work. Schematic describing the experimental procedure followed: (a) amyloid fibrils were first produced by self-assembly of denatured β-lactoglobulin monomers; (b) using different stirring speeds at ambient conditions, the amyloid fibrils were shortened into rods of different aspect ratios (c). The scale bar of 3 μm applies to all images.

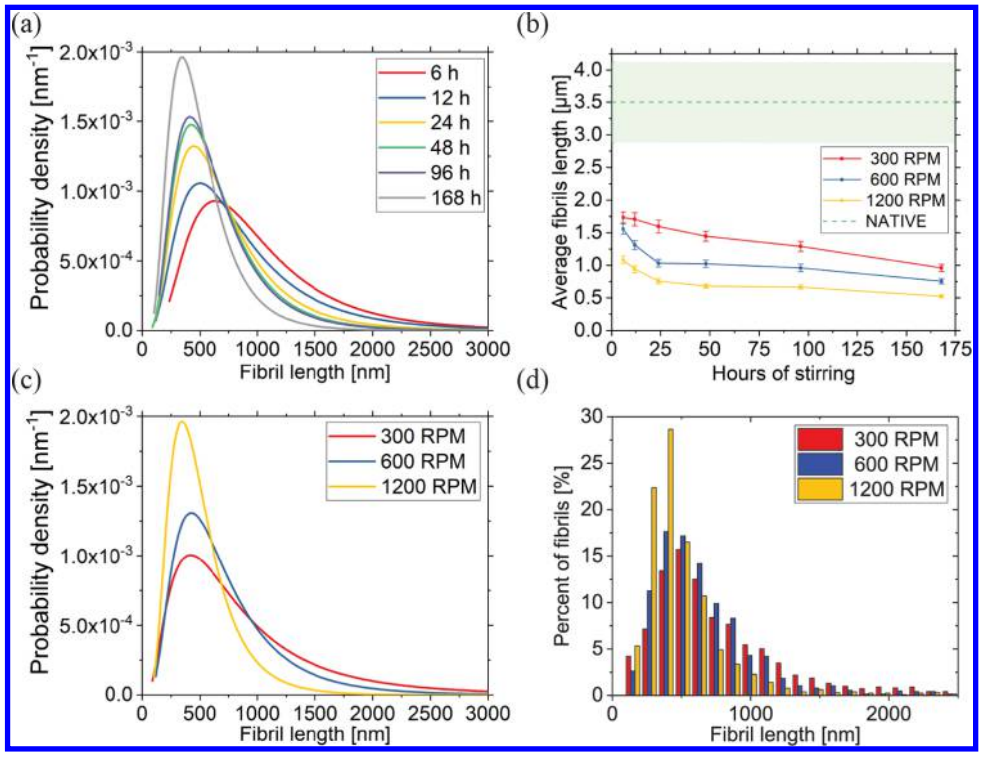

Figure 2. Characterization of fibril length distributions *via* statistical analysis of AFM images. (a) Contour length distribution of the amyloid fibrils shortened at 1200 rpm, fitted by a log-normal distribution function after different stirring times. (b) Arithmetic average fibril length after different stirring times and speeds. (c–d) Final fibril length distributions after 1 week of stirring for the three speeds investigated, plotted as fitted log-normal distributions (c) and original histograms (d). The fitting parameters of the log-normal distributions are given in the Supporting Information (SI).

remained the only liquid crystalline phase associated with this system. Very recently, however, cholesteric liquid crystals have also been discovered in this class of biocolloids in a narrow range of particle properties and environmental conditions.[27] β-lactoglobulin amyloid fibrils suspensions are a particularly interesting (and challenging) model system for elucidating the liquid crystalline phase behavior of chiral rod-like colloidal suspensions, due to their high persistence length (1980 nm), large aspect ratio, and well-defined chirality at the single fibril level.[22,28] Amyloid fibrils can be assembled into rods with different structural properties by fine-tuning the fibrillization process[29] and can be shortened and homogenized using

DOI: 10.1021/acsnano.8b07557
ACS Nano XXXX, XXX, XXX−XXX

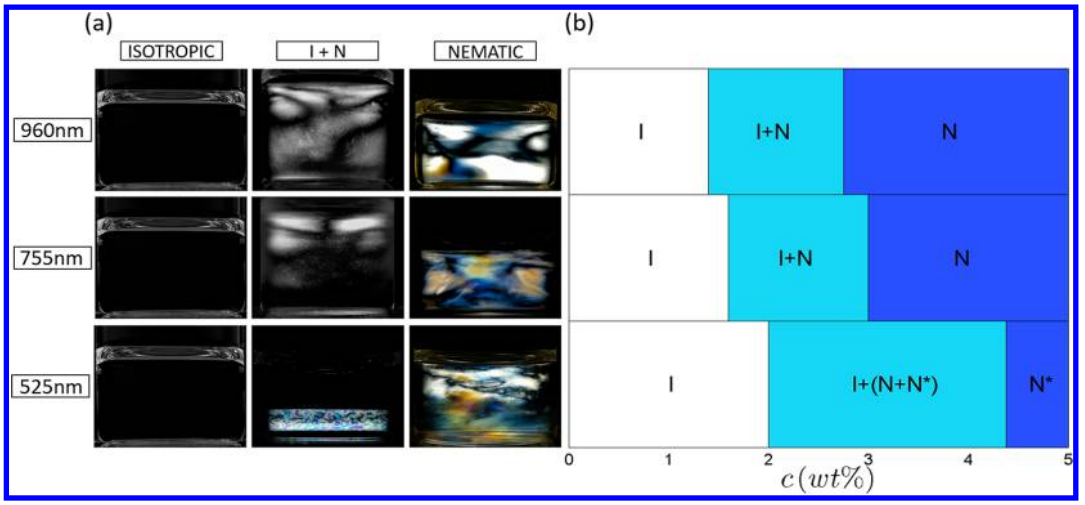

Figure 3. Amyloid fibril phase diagrams for suspensions of various fibril aspect ratios. (a) Photographs of the samples taken between cross polarizers showing the dispersions in the isotropic phase (left), in the coexistence I + N phase (center), and in the completed nematic phase (right). (b) Corresponding phase diagrams plotted against fibril concentration for the three different fibrils lengths. I, N, and N* stand for isotropic, nematic and chiral nematic, respectively.

mechanical stresses.[30] The few chiral biocolloid models previously used to study the effect of rod length on the liquid crystalline behavior, such as viruses, DNA, and actin filaments, imply genetic engineering[31−33] or chemical modifications,[34] thus limiting the number of possible achievable lengths and inducing changes in sequence and linear charge densities, which may affect the final liquid crystalline structures.[35] In this work, amyloid fibrils, self-assembled from native β-lactoglobulin protein, were cut into rod-like particles with different characteristic contour lengths using mechanical stirring at different rotation speeds (Figure 1), allowing to isolate the effect of the rod aspect ratio on the amyloid phase behavior. This tunability of the rods structural parameters offers the possibility to further elucidate the relationship between the microscopic parameters of the hard rod-like particles and the resulting phase behavior of the ensued liquid crystalline phases.

RESULTS AND DISCUSSION

Tuning Amyloid Fibrils Contour Length Distribution. In order to study the effect of fibrils contour length on the resulting liquid crystalline phase behavior, dispersions containing amyloid fibrils with different contour lengths were produced by cutting the mature, native fibrils (contour length 1−20 μm) using different hydrodynamic shear forces imposed by a magnetic stirring bar (Figure 1). This method allowed obtaining fibrils with fixed diameter (controlled by the initial fibrillation conditions)[28] but different contour lengths. For all the samples considered hereafter, the final average contour length of the fibrils L_c was well below their persistence length (L_p= 1980 nm).[28] Figure 2a shows the length distribution of the fibrils after different stirring times for the constant stirring speed of 1200 rpm. With increasing duration of stirring, the average contour length of the fibrils decreases and the length distribution becomes narrower, leading to homogenization in length of the fibrils. To produce fibrils of different contour lengths, different stirring speeds were furthermore used: 1200, 600, and 300 rpm. After 1 week of stirring, the average fibril lengths in the samples were 525, 755, and 960 nm with polydispersity indices (PDIs) equal to 1.55, 1.85, and 2.04 for stirring speeds of 1200, 600, and 300 rpm, respectively. Thus, for comparable stirring durations, a higher stirring speed allows obtaining shorter fibrils and narrower length distributions. The effect of stirring speeds and time on the average contour length of the fibrils is shown in Figure 2b. These data reveal an initial rapid decrease in length (within the first 10 h), followed by a more gradual decrease from 1 day up to 7 days, after which the stirring was stopped. The final length distribution of the fibrils after 1 week of stirring is displayed as original data histograms (Figure 2d) and their corresponding log-normal fits to data distribution (Figure 2c).

Amyloid Fibrils Contour Length Controls Phase Behavior. Dilute colloidal suspensions of amyloid fibrils are isotropic and show no birefringence when viewed under polarized light between crossed polarizers. For concentrations above a certain critical threshold C_i, birefringent anisotropic domains start to nucleate and grow, eventually leading to a bulk anisotropic phase. To build the phase diagram for each contour length, the fibrils suspensions were first concentrated until the solutions appeared completely birefringent through cross polarizers, thereby reaching the critical concentration for a complete nematic phase C_n. The solution was then diluted until complete extinction of birefringence (isotropic phase) in order to find the exact value of C_i (Figure 3a). Between these two critical concentrations, the samples showed a biphasic behavior characterized by the formation of nematic droplets, known as tactoids, surrounded by an isotropic phase, demonstrating that the thermodynamic phase transition is of the first-order type (Figure 3). After three months of equilibration, the sample containing the shortest fibrils showed a clear phase separation due to the sedimentation of the tactoids. The macroscopic phase separation allowed measuring the concentrations of both phases at completed equilibration. On the other hand, after similar equilibration times, the sample containing tactoids of longer fibrils never reached macroscopic phase separation. The reasons may be both of kinetic origin, possibly due to the higher viscosity of the medium that prevents sedimentation of the tactoids,[36] or of thermodynamic origin, as a much narrower coexistence region of the isotropic + nematic phase for longer rods implies a lower difference in compositions (and thus densities) for the coexisting isotropic and nematic phases.[37]

DOI: 10.1021/acsnano.8b07557
ACS Nano XXXX, XXX, XXX−XXX

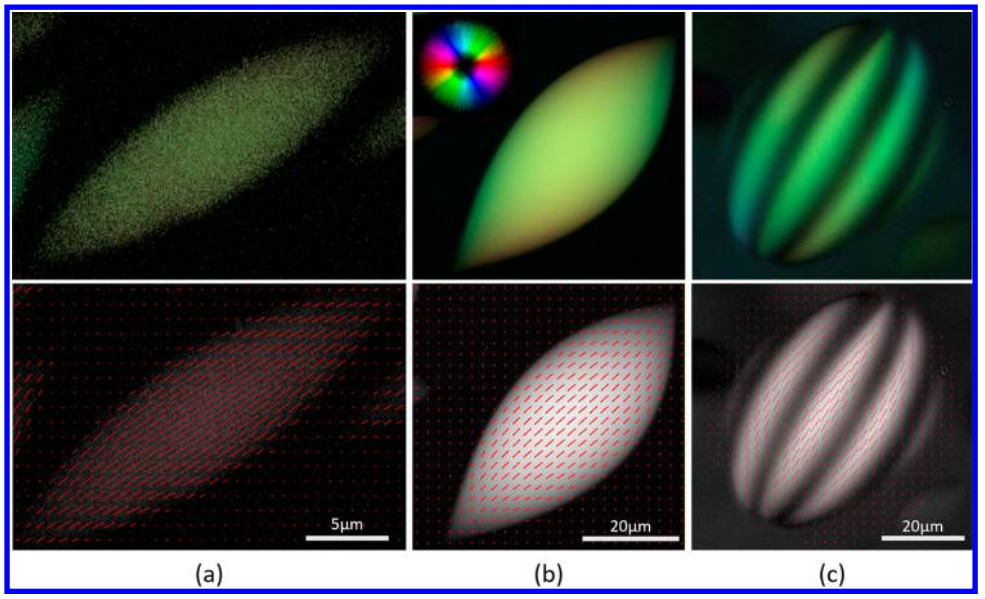

Figure 4. Classification of different tactoid types. The three classes of tactoids identified showing homogeneous (a), bipolar (b), and cholesteric (c) director field analyzed with LC PolScope (color map first row and their relative director field in the second row).

The critical concentrations at the bifurcation characterizing the isotropic−nematic phase transition for rigid rods of contour length L and diameter D, as predicted by the Onsager theory, depend on the rods' aspect ratio, $\phi \sim \frac{D}{L}$ and therefore C_i and C_n are shifted to higher values when the fibrils in solution are shorter.[23,37,38] When the rods are charged and electrostatic effects are to be accounted for, the real diameter D is typically replaced by (D^2/D_{eff}), where $D_{eff} = D + k^{-1}(\ln A + C + \ln 2 - 1/2)$ is the effective diameter inclusive of double layers electrostatic effects, k^{-1} the Debye length, C the Euler's constant, and $A = 2\pi\nu_{eff}^2 k^{-1} Q \exp(-kD)$, with ν_{eff} being the linear charge density and Q the Bjerrum length (≈0.7 nm in water at room temperature).[23] Considering the charge density and electrostatic effects of ionic strength and counterion concentration, an effective diameter[23] of 4.08 nm is found, a value very close to the physical diameter of 4 nm[28] (details in SI).

Accordingly, the sample containing the longest fibrils (L_c = 960 nm) showed a nematic transition at a concentration, C_i, of 1.4 wt %, lower than for the medium (L_c = 755 nm) and the short (L_c = 525 nm) fibrils systems, which showed an isotropic−nematic transition at 1.6 and 2 wt %, respectively. Similarly, the concentration for a completed nematic transition, C_n, was lower for the longest fibrils (2.7 wt %) than for the medium (3 wt %) and shortest (4.3 wt %) fibrils. These concentration values estimated from experiments fit well the theoretical predictions from the classic Onsager theory. Following this theory and considering a fibril density[39] of ∼1.3 g/cm^3, the lower critical concentration lies at $\phi \sim 3.34\frac{D^2}{D_{eff}L}$ corresponding to concentrations of 1.8, 2.3, and 3.2 wt %. The upper critical concentration is predicted to be at $\phi \sim 4.49\frac{D^2}{D_{eff}L}$ corresponding to 2.4, 3.0, and 4.3 wt %, in excellent agreement with the experimental observations.

The widths of the coexistence windows are also affected by the rods length, as predicted by the Onsager theory based on the aspect ratio dependence of both the lower and the upper transitions. Accordingly, samples with the shortest fibrils also present the widest I + N coexistence region (Figure 3b). Most importantly, an extensive optical microscopy analysis showed that only the system containing the shortest fibrils developed a cholesteric phase (referred as N*), which is discussed at length in the following section. In the lowest row of Figure 3b (shortest fibrils with L_c = 525 nm), the coexistence region labeled as I + (N + N*) is not to be understood as a triphasic region but as a biphasic region only: We have shown very recently that the N → N* transition is spontaneous when a critical size of the tactoid is reached and the transition is simply controlled by the tactoid size for a given system.[27] Thus, in the present study, conclusions on the nature of the tactoids are drawn by paying particular attention to compare tactoids of the same size.

Effect of Fibril Length on the Nematic and Cholesteric Phase Transitions. All fibril systems, when mixed at concentrations within the isotropic−nematic coexistence region of the phase diagram, nucleate from the isotropic phase, anisotropic birefringent tactoids that grow with time. The tactoids with smallest volume are homogeneous nematic tactoids, characterized by a highly elongated shape, that is a high aspect ratio between the long and small axes of the tactoids and a director field always parallel to the long axis of the tactoid. When a critical volume is reached, the homogeneous tactoids change morphology, turning into bipolar nematic tactoids, characterized by a director field that follows the interface of the droplet and a decrease in the tactoid aspect ratio. On further increase of the volume, cholesteric tactoids start to emerge. This last class of tactoids is characterized by the lowest aspect ratio approaching one, that is, they are nearly spherical, and exhibit a typical striped texture, caused by the periodic rotation of the director along a direction perpendicular to the long axis of the tactoid.[40,41] All of these observations on the size-dependent morphologies, the progressive decrease in aspect ratio and liquid crystalline nature of the tactoids are in agreement with our recent findings on tactoids of different volumes generated by a single-contour length amyloid fibrils distribution.[27] LC PolScope imaging of the various tactoids was used to follow the evolution of the

DOI: 10.1021/acsnano.8b07557
ACS Nano XXXX, XXX, XXX−XXX

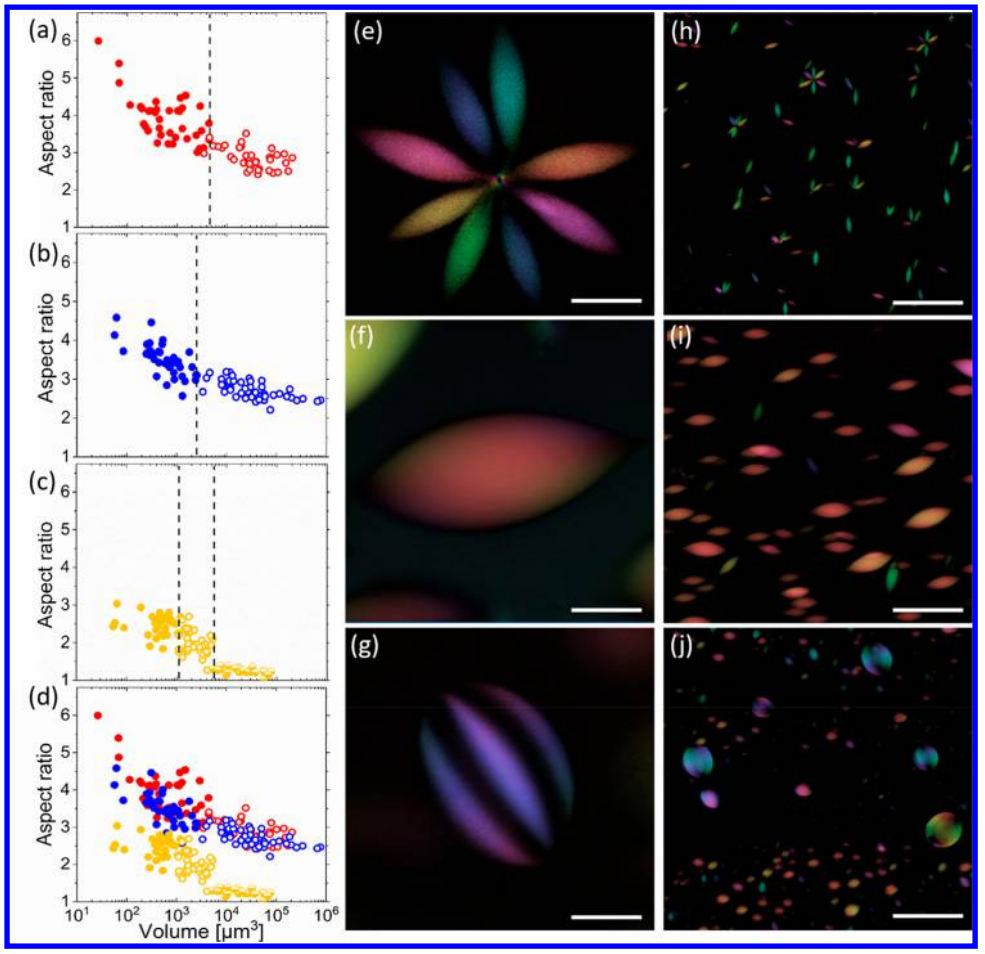

Figure 5. Amyloid fibrils length effects on their liquid crystalline structures. Plots showing the aspect ratio of the tactoids as a function of their volumes in the suspension containing long (a), medium (b), and short (c) amyloid fibrils (full dots indicate homogeneous tactoids, empty dots bipolar and the half-empty dots in (c) the cholesteric ones). The dashed lines represent the estimated critical volume for the transitions. The three plots are merged together in panel (d) for comparison. LC PolScope color maps images showing the peculiar structures for the three length distributions: (e) a flower-like structure formed by homogeneous tactoids in the solution containing long fibrils, (f) a bipolar nematic tactoid formed in the solution of medium fibrils, and (g) a cholesteric tactoid formed in the sample containing short fibrils (scale bars equal to 15 μm). In the third column, overviews of the three solutions in the I + N are presented (scale bar is 200 μm) to highlight the different configurations in tactoids of similar volumes, depending on rod length.

director field, allowing unambiguous assessment of the morphology. A selection of representative images of the three major classes of tactoids formed in the biphasic region of the phase diagram, along with the director field orientation, is shown in Figure 4.

As summarized in Figure 5, the different characteristic lengths of the rods in the three systems have a strong influence on the types of liquid crystal structures that are nucleated in the I + N phase. In particular, three major effects can be noted. Beside the continuous decrease in aspect ratio with increasing volume observed in all the tactoids already mentioned (Figure 5a–c), the first notable effect is the correlation between rods length and tactoid aspect ratio (Figure 5d). At a given volume, in the system composed by the longest rods, the aspect ratios of the homogeneous and bipolar tactoids are generally larger than those observed for the medium and for the shortest rods. These results indicate that when the rods are shorter, the tactoid assumes a more spheroidal shape (see also Figures S2 and S3).

In the case of homogeneous tactoids, the origin of the decrease in aspect ratio with fibrils length may have a subtle origin. Indeed, for a homogeneous distribution of the director field, the splay and elastic energy contributions are essentially zero, and thus the energy is dominated by the surface anchoring contribution only. It has been shown before that the aspect ratio in this case scales in a nontrivial, yet monotonically increasing way with the anchoring strength.[41] As better discussed later, the latter is expected to be an increasing function of the contour length, and therefore this explains, at least qualitatively, a decrease in the aspect ratio with a decrease of the amyloid contour length in the case of a homogeneous nematic distribution.[41]

For the tactoids in a bipolar configuration, this effect has an immediate intuitive foundation: Rods inside the tactoids tend to align following both the nematic director and the interface (parallel anchoring), so that the shorter the rods, the higher the curvature that the interface can sustain without introducing strong deformation. On a more quantitative basis, the splay and bend elastic moduli weighting the two main bulk energy contributions of the tactoids scale linearly with the contour length,[42,43] so that in the case of shortened amyloid fibrils, their progressive softening with decreasing fibril contour lengths explains why shorter amyloid lengths may afford, energetically, a higher curvature of the tactoids.

DOI: 10.1021/acsnano.8b07557
ACS Nano XXXX, XXX, XXX–XXX

A recurring and intriguing structure found in the solution containing the longest rods consists in the formation of a "flower-like" array of homogeneous and bipolar tactoids radially arranged around a common nucleation point (Figure 5d and Figure S5). This structure was found only in the sample containing longer rods, probably due to destruction of the nucleation points during the stirring process with higher speeds. A possible explanation is that only the longer fibrils produce entanglement points from which these flower-like defects nucleate radially, although further investigations are necessary to shed light into this supracolloidal form of organization.

The second important finding regards the values of the adimensional anchoring strength calculated by analyzing the homogeneous tactoids formed in the three different solutions; more specifically, the anchoring strength was found to increase linearly with increasing rod length. These conclusions were drawn based on three different methods and considerations. To start, the anchoring strength is known to be function of the angle between the main axis of the tactoid and the surface tangent taken at either pole (the tip angle ϑ, constant in homogeneous nematic tactoids).[41] More precisely, following the Wulff model, the adimensional anchoring strength can also be expressed as $\omega = 1 + (\tan(\vartheta))^{-2}$. The angle ϑ was experimentally found to decrease with increasing rod length, moving from 44° in tactoids composed by short rods to 40° and 36° for medium and long rods respectively (Figure 6b–d).

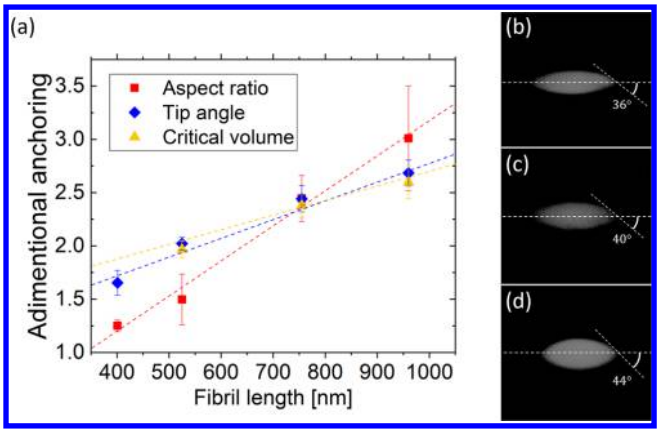

Figure 6. Adimensional anchoring strength as linear function of fibril length. Panel (a) shows the linear dependence of the adimensional anchoring strength and the rod length. The red symbols correspond to the values calculated by measuring the aspect ratio, the blue symbols correspond to the ones calculated measuring the tip angle, while the yellow ones correspond to the scaling estimation based on the critical radius of the homogeneous-bipolar transition (the linear fit in dashed line). The points corresponding to amyloids with length 401 nm were calculated using the tactoids shown in Nystrom *et al.*[27] LC Polscope images illustrating the tip angle ϑ measurements on homogeneous tactoids composed by rods of 960 (b), 755 (c), and 525 nm (d).

In addition, the Wulff model suggests that, when $\omega > 1$, the anchoring strength should be related to the aspect ratio α of homogeneous tactoids *via* $\omega = \left(\frac{\alpha}{2}\right)^2$, yielding anchoring values in excellent agreement with the ones calculated using the tip angle expression. The anchoring strength calculated as such for the three amyloid rod lengths, is further completed by the anchoring strength of amyloids rod length of 401 nm, by applying the same two methods (tip angles and aspect ratios) on the homogeneous tactoids published by Nystrom *et al.*[27] By proceeding as above, both tip angle and aspect ratio methods provide results in very good agreement, both confirming a linear evolution of ω with L (Figure 6).

In order to support the experimentally observed linear evolution of the adimensional anchoring strength with rod length, we also provide a simple scaling consideration. It is known[27] that the critical volume for the homogeneous to bipolar transition scales, as a first approximation, as $\frac{V_{cr}}{\alpha} \sim \left(\frac{K}{\gamma\omega}\right)^3$, where V_{cr} represents the critical volume $\approx r^2R$ or $\approx r^2\alpha r$, with α the aspect ratio, K is the average Frank elastic constant, following the one constant assumption, γ is the isotropic–nematic interfacial tension, and ω is the anchoring strength. A slightly more accurate expression for this transition distinguishing between splay and bending elastic constants, which is found in the Supporting Information of ref 27, leads to the same qualitative conclusions, and it is therefore omitted here for sake of simplicity. The tactoid critical radius for the homogeneous-bipolar transition scales therefore as $r_{cr} \sim \frac{K}{\gamma\omega}$. The elastic constant K scales[44] as $K \sim K_B T \phi_N \left(\frac{L}{D^2}\right)$ while the surface tension is approximately equal to $\gamma \approx b\frac{K_B T}{LD}$, where K_B is Boltzmann constant, T the temperature, ϕ_N the volume fraction of amyloid in the nematic tactoid (accessible from the upper bifurcation compositions in Figure 3b), and b a constant equal to 0.6 for amyloid fibrils.[27,45] Thus, using $\omega(L) \sim \frac{K(L)}{\gamma(L) r_{cr}(L)}$ or, which is equivalent, $\omega(L) = c\frac{K(L)}{\gamma(L) r_{cr}(L)}$, with c a numerical factor, we are able once again to evaluate, using accessible experimental input variables, how the anchoring strength varies with the rod length. By using the $r_{cr}(L)$ measured in the homogeneous tactoids nearest to the bipolar transition volume and the three available ϕ_N from the upper bifurcation compositions in Figure 3b, we find again that the anchoring strength increases linearly with increasing rod length (Figure 6 and Figure S4; $c = 4$). The values of ω calculated with the three different methods are in the same order of magnitude of the one recently calculated for carbon nanotubes of a fixed length.[46]

With accurate values of the adimensional anchoring strength available, further considerations become possible also on the bipolar-cholesteric transition. In Nystrom *et al.*[27] it was proposed, by scaling arguments on the Frank–Oseen energy functional that such a transition occurs at $\frac{V}{\alpha} \approx \left(\frac{2\gamma\omega}{\alpha^2 K_2 q^2}\right)^3$, where K_2 is now the twist constant and $q = 2\pi/p$ with p the pitch of the cholesteric phase. Nonetheless, in the lack of accurate values of the adimensional anchoring strength, a simpler form was also derived in the same work by combining the same energy arguments with a scaling form of the anisotropic surface tension, concluding that in the limit of $L \gg D$ and spheroidal cholesteric droplets, the bipolar-cholesteric transition should be observed at $\frac{V}{\alpha} \approx \left(\frac{2\gamma \times 0.85}{K_2 q^2}\right)^3$, which is identical to the former, except for the 0.85 value replacing the ω/α^2 factor. In order for the two expressions to be equivalent, one must have $\omega/\alpha^2 \approx 0.85$, which can now be experimentally verified. Indeed, by taking the averages of anchoring strength and aspect ratio of the bipolar tactoids at the bipolar-

DOI: 10.1021/acsnano.8b07557
ACS Nano XXXX, XXX, XXX–XXX

cholesteric transition, we have $\omega = 1.45$ and $\alpha = 1.3$ for the 401 nm rods in ref 27 and $\omega = 1.8$ and $\alpha = 1.45$ for the 525 nm rods, immediately obtaining $\omega/\alpha^2 \approx 0.85$ in both cases and thus validating the equivalence between the two expressions proposed by Nystrom *et al.*[27] Note the difference between $\omega/\alpha^2 = 0.85$ at the bipolar-cholesteric transition and $\omega/\alpha^2 = 0.25$ for homogeneous tactoids suggested by the Wulff model arises from the different aspect ratios α in homogeneous (highly elongated) and cholesteric (spheroidal) tactoids.

In Nystrom *et al.*,[27] the cholesteric pitch p_{401} of fibrils with $L_c = 401$ nm has been estimated to be of 20 μm, and in the present study, we measured the cholesteric pitch for $L_c = 525$ nm finding $p_{525} = 15$ μm. Therefore, another key finding of the present study is that the pitch of cholesteric phase decreases on increasing fibrils length for dispersions of longer fibrils. We also measured the nematic order parameter S for these two cases $S_{401} = 0.45$ and $S_{525} = 0.49$ (see SI for details about the experimental procedure used for measuring the order parameter). To rationalize the pitch dependence on fibril length, we designed a very simple model of amyloid fibrils, as shown in Figure 7a, which we used to calculate the pitch

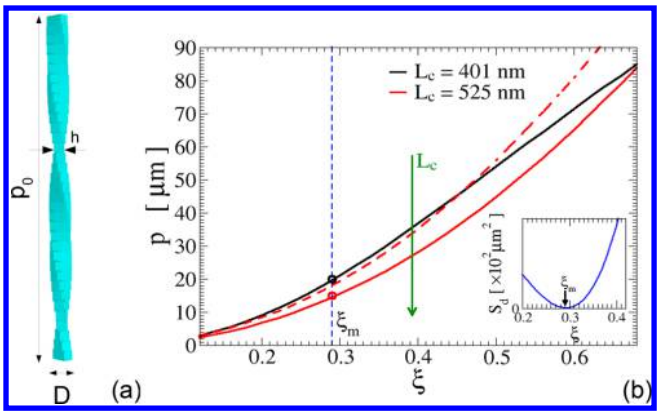

Figure 7. Theoretical estimate of pitch variation. (a) Model of amyloid fibrils used in theoretical calculations: Each fibril is represented as a twisted set of parallelepipeds with pitch $p_0 = 70$ nm, diameter $D = 4$ nm, and thickness $h = 2$ nm. Note that over a length equal to the pitch p_0, there are 35 parallelepipeds, so that the height of each box along the symmetry axis of the fibril is 2 nm. (b) Theoretical pitch as a function of the parameter ξ for amyloid fibrils of average lengths 401 and 525 nm. The inset shows the sum of least squared residuals S_d as a function of ξ, where the minimum ξ_m is also indicated. Along the vertical dashed line in the main panel, whose abscissa corresponds to ξ_m, the experimental values of the pitch are shown. Dashed red line corresponds to fibrils of 525 nm, where in the theoretical calculations we keep fixed the value of α_N to the value for fibrils of 401 nm.

according to the theory developed in refs 33 and 47 (see SI for more details). Note that our coarse-grained model accounts for steric hindrance of fibrils composed of two filaments, that is, the most crowded population of fibrils according to the experimental results reported by Adamcik *et al.*[28]

The flexibility of the fibrils enters into the theoretical calculation of the pitch through a characteristic length L_0, which discriminates the two regimes of stiff and fully flexible fibrils. According to ref 48, L_0 has to be related to the deflection length $\lambda = \frac{L_p}{\alpha_N}$ and, thus, we set $L_0 = \xi\lambda = \frac{\xi L_p}{\alpha_N}$, where $\alpha_N = \alpha_N(S)$ is the Onsager parameter and ξ is an adjustable parameter. Within this approach, given the fibril length distribution and the nematic order parameter (which are known experimentally), the pitch is solely a function of ξ. In Figure 7b the theoretical pitch p^{th}_{401} for $L_c = 401$ nm and p^{th}_{525} for $L_c = 525$ nm is shown as a function of ξ. An optimal value of ξ can be estimated by minimizing the sum of the least squared residuals $S_d(\xi) = (p^{th}_{401}(\xi) - p_{401})^2 + (p^{th}_{525}(\xi) - p_{525})^2$. $S_d(\xi)$ is shown in the inset of Figure 7b, and it can be seen that the optimal value ξ_m is approximately equal to 0.29.

The theory captures very well the variation of the pitch, which roughly amounts to 30%. This variation can be mostly ascribed to the decrease of the deflection length on increasing α_N, which enhances the effect of bending fluctuations, thus effectively making the fibrils more flexible (see Figure 7) and may bear a general validity. Indeed, Odijk first observed[48] that for PBLG chiral nematic polymers at a fixed concentration, the pitch reduces on increasing the molecular weight due to the role played by bending fluctuations, although the molecular weight dependence of the pitch could not be quantitatively predicted by his scaling approach. Similar findings were also reported by Grelet and Fraden on filamentous viruses, again, however, without a theoretical interpretation capable to explain the observed findings.[16] The increase of nematic ordering at coexistence on increasing the fibril length can be also interpreted as an effect of bending fluctuations. According to eqs (IX.5) in ref 49, which are valid for semiflexible polymers (*i.e.*, when the contour length is much greater than λ), the value of S at coexistence has to increase on increasing the contour length of the nematogen.

The last key finding of the present study is that the cholesteric phase is only observed in the dispersion containing the shortest fibrils ($L_c \leq 525$ nm). To rationalize this observation, we aim at estimating the ratio $\Gamma = \frac{K}{\Delta F}$, where K is the thermal energy and ΔF is the typical free energy barrier associated with cholesteric minima in the free energy landscape. We expect that the cholesteric phase is destabilized in favor of the nematic phase if $\Gamma > \Gamma_0$. We now observe that the elastic contributions to the free energy of a cholesteric droplet of volume V are expected to roughly scale as $k_B T c_m^2$ (c_m is the mass concentration of fibrils, see also eqs 3 and 4 in the SI), and they are much smaller than the contributions of the undeformed nematic phase.[33] Hence, we assume that $\Delta F \propto k_B T c_m^2$. From the equipartition theorem of energy one has that $K \propto \nu \frac{N}{2} k_B T$, where ν are the internal degree of freedom of each semiflexible fibrils and N the number of fibrils in the volume V (*i.e.*, $N \propto c_m$). Due to bending fluctuations, each fibril can be thought as a set of $\frac{L_c}{\lambda}$ independent fragments, so that $\nu \propto \frac{L_c}{\lambda}$. From such a simple scaling, it follows that $\Gamma \propto \alpha_N L_c / c_m L_p$ so that it increases for longer fibrils, for which c_m is smaller and both L_c and α_N are larger. In conclusion, we reason that at the low concentrations of long fibril dispersions (*i.e.*, for $L_c >$ 525 nm), the condition $\Gamma > \Gamma_0$ is fulfilled, thus destabilizing the cholesteric phase in favor of the nematic.

CONCLUSIONS

By systematically shortening the contour length of amyloid fibrils *via* mechanical shear stresses, we have shown the pivotal role of fibrils length on the shape and nature of the ensued liquid crystalline phases. When the amyloid suspensions are mixed within the region of the phase diagram characterized by the coexistence of isotropic and nematic phases, tactoid

DOI: 10.1021/acsnano.8b07557
ACS Nano XXXX, XXX, XXX−XXX

droplets nucleate and grow from an initially isotropic continuous phase. The concentration boundaries of this isotropic and nematic coexistence region agree well, for all the systems considered, with the theoretical predictions of the Onsager theory for hard rods. More importantly, the equilibrium shapes of the tactoids formed in this biphasic regime show a direct correlation with the contour lengths of the amyloid fibrils investigated. Specifically, the decrease in amyloid fibrils contour length induces a sequence of transitions from homogeneous tactoids to bipolar tactoids to cholesteric droplets on decreasing the average contour length of the fibrils, with the homogeneous-bipolar transition occurring at a specific critical volume value that decreases with decreasing rod length. These differences in the critical volumes together with the tactoids specific critical radiuses and tip angle values allowed proving a linear dependence of the anchoring strength with the rod length.

A key finding of the present work is that the emergence of a cholesteric phase in these systems becomes possible only when the fibrils are shortened below a critical threshold length and that below this length, the cholesteric pitch increases upon further shortening of the fibrils. Both effects are duly captured by theoretical considerations accounting for the increasing role of the bending fluctuations and the simultaneous decrease of the energy barrier separating the cholesteric and nematic phases over the thermal energy, when the fibril contour length grows.

The possibility of controlling the contour length of the amyloid fibrils by simple shear stresses can be achieved for these biological chiral rod-like colloids and provides a versatile and facile tool for tuning the resulting liquid crystalline phases, as exemplified in this work by the very rich phase diagram inclusive of homogeneous, bipolar, and cholesteric tactoids. Hence, amyloid fibrils of controllable contour length are anticipated to become a valuable model system to test some of the predictions of the most advanced soft condensed matter theories on colloidal liquid crystals.

MATERIALS AND METHODS

Samples Preparation. β-Lactoglobulin was purified from whey protein according to the protocol described by Vigolo *et al.*[50] To produce amyloid fibrils, 300 mL of 2 wt % β-lactoglobulin solution was adjusted to pH 2 and incubated at 90 °C for 5 h. During the heating process, the solution was stirred using a magnetic bar at 150 rpm. To stop the aggregation process, the flask was immediately cooled by immersion into an ice−water mixture. β-Lactoglobulin amyloid fibrils with different contour lengths were obtained by stirring preformed native amyloid fibrils for 1 week. In these experiments, 100 mL of native fibril dispersion were subjected to three different shearing rates, imposed by stirring at 300, 600, and 1200 rpm using magnetic bars. The dispersions were thereafter dialyzed against pH 2 adjusted Milli-Q water using a semipermeable membrane (Spectra/Por dialysis membrane 1, MWCO 100 kDa) for 4 days and then up concentrated with reverse osmosis against a pH 2 and 5 wt % PEG (MW 35 kDa) solution (Spectra/Por dialysis membrane 1, MWCO 6−8 kDa).

Atomic Force Microscopy Characterization. One mL sample aliquots were taken after 6, 12, 24, 48, 72, 96, 168 h of stirring for AFM analysis. The fibril samples were diluted in pH 2 Milli-Q water into a final concentration of 0.01 wt %, and then 20 μL solution were deposited onto freshly cleaved mica, incubated for 2 min, rinsed with Milli-Q water, and dried with compressed air flow. AFM experiments were performed using a Multimode VIII scanning probe microscope (Bruker, USA), and images were acquired in tapping mode at ambient conditions. The average contour lengths of amyloid fibrils and the corresponding contour length distributions were obtained using the open source code FiberApp.[51]

Phase Diagram Determination. To investigate the phase behavior, the fibril dispersions were up concentrated until a fully nematic phase was achieved without crossing the sol/gel transition. Solutions with different concentrations were then prepared with progressive dilution and mixing using pH 2 Milli-Q water (with dilution steps of 0.1 wt %) down to concentrations where the samples were completely isotropic. The absence of birefringence domains was investigated first between cross polarizers and then after equilibration with polarized microscopy.

Optical Microscopy/Cross-Polarizers. The macroscopic features of liquid crystalline ordering in the samples were first studied between cross-polarizers to determine the presence of birefringence. To confirm the macroscopic observation and further analyze the liquid crystal structures, glass cuvettes (0.2 × 4 × 40 mm^3, VitroTubes, Vitrocom) were filled with samples after mixing using a pipet, sealed with epoxy, and imaged with optical microscope. The cuvettes were examined after 24 h of equilibration with a cross-polarized microscope, and a LC-PolScope universal compensator was used to examine the orientation of the amyloids inside the structures formed in the isotropic−nematic coexisting phase.

ASSOCIATED CONTENT

Supporting Information

The Supporting Information is available free of charge on the ACS Publications website at DOI: 10.1021/acsnano.8b07557.

Length characterization details for the log-normal distributions of the three stirring speeds. Rod length effects on tactoid shape and detailed LC PolScope images. Anchoring strength derivation. Flower-like structure formation, AFM images of nucleation points, and LC Polscope images of different stages of tactoids formation. Theoretical framework to predict a cholesteric pitch dependence on the amyloid contour length (PDF)

AUTHOR INFORMATION

Corresponding Author

*E-mail: raffaele.mezzenga@hest.ethz.ch.

ORCID

Massimo Bagnani: 0000-0002-1326-1600
Gustav Nyström: 0000-0003-2739-3222
Cristiano De Michele: 0000-0002-8367-0610
Raffaele Mezzenga: 0000-0002-5739-2610

Author Contributions

M.B. carried out the experiments, analyzed data, and interpreted the results. G.N. contributed experiments and results analysis and interpretation. C.D.M. developed the theoretical formalism describing the length dependence of the cholesteric pitch and contributed to the physical scaling arguments. R.M. developed the physical scaling arguments, analyzed and interpreted the results, and designed and directed the study. All authors discussed the results and contributed to writing.

Notes

The authors declare no competing financial interest.

ACKNOWLEDGMENTS

We acknowledge support of T. Schwarz from the Scientific Center for Optical and Electron Microscopy of ETH Zurich (ScopeM) for help with the laser scanning confocal microscopy experiments. The authors gratefully acknowledge

DOI: 10.1021/acsnano.8b07557
ACS Nano XXXX, XXX, XXX−XXX

Mario Arcari, Paride Azzari, Yiping Cao, Michael Diener, Ilya Savchenko, Mattia Usuelli, Salvatore Assenza, and Paul van der Schoot for valuable discussions on the experiments and results. Funds from ETH Zurich (SEED-43 16 1) are gratefully acknowledged.

REFERENCES

(1) Lekkerkerker, H. N. W.; Vroege, G. J. Liquid Crystal Phase Transitions in Suspensions of Mineral Colloids: New Life from Old Roots. *Philos. Trans. R. Soc., A* **2013**, *371*, 20120263.
(2) Vroege, G. J.; Lekkerkerker, H. N. W. Theory of Phase Separation for a Solution of Tridisperse Rod-like Particles. *Colloids Surf., A* **1997**, *129−130*, 405−413.
(3) Mitov, M. Cholesteric Liquid Crystals in Living Matter. *Soft Matter* **2017**, *13*, 4176−4209.
(4) Dierking, I.; Al-Zangana, S. Lyotropic Liquid Crystal Phases from Anisotropic Nanomaterials. *Nanomaterials* **2017**, *7*, 305.
(5) Rey, A. D. Liquid Crystal Models of Biological Materials and Processes. *Soft Matter* **2010**, *6*, 3402.
(6) Giraud-Guille, M. M.; Besseau, L.; Martin, R. Liquid Crystalline Assemblies of Collagen in Bone and *in Vitro* Systems. *J. Biomech.* **2003**, *36*, 1571−1579.
(7) Romano, P.; Fabritius, H.; Raabe, D. The Exoskeleton of the Lobster Homarus Americanus as an Example of a Smart Anisotropic Biological Material. *Acta Biomater.* **2007**, *3*, 301−309.
(8) Diah, S. Z. M.; Karman, S. B.; Gebeshuber, I. C. Nanostructural Colouration in Malaysian Plants: Lessons for Biomimetics and Biomaterials. *J. Nanomater.* **2014**, *2014*, 1.
(9) Lagerwall, J. P. F.; et al. Cellulose Nanocrystal-Based Materials: From Liquid Crystal Self-Assembly and Glass Formation to Multifunctional Thin Films. *NPG Asia Mater.* **2014**, *6*, e80.
(10) Schütz, C.; Agthe, M.; Fall, A. B.; Gordeyeva, K.; Guccini, V.; Salajkova, M.; Plivelic, T. S.; Lagerwall, J. P. F.; Salazar-Alvarez, G.; Bergström, L. Rod Packing in Chiral Nematic Cellulose Nanocrystal Dispersions Studied by Small-Angle X-Ray Scattering and Laser Diffraction. *Langmuir* **2015**, *31*, 6507−6513.
(11) Finkelmann, H.; Kim, S. T.; Muñoz, A.; Palffy-Muhoray, P.; Taheri, B. Tunable Mirrorless Lasing in Cholesteric Liquid Crystalline Elastomers. *Adv. Mater.* **2001**, *13*, 1069−1072.
(12) Saito, M.; Uemi, H. A Spatial Light Modulator That Uses Scattering in a Cholesteric Liquid Crystal. *Rev. Sci. Instrum.* **2016**, *87*, 33102.
(13) Frka-Petesic, B.; Guidetti, G.; Kamita, G.; Vignolini, S. Controlling the Photonic Properties of Cholesteric Cellulose Nanocrystal Films with Magnets. *Adv. Mater.* **2017**, *29*, 1701469.
(14) Kohlstedt, K. L.; Solis, F. J.; Vernizzi, G.; De La Cruz, M. O. Spontaneous Chirality *via* Long-Range Electrostatic Forces. *Phys. Rev. Lett.* **2007**, *99*, 030602.
(15) Barry, E.; Hensel, Z.; Dogic, Z.; Shribak, M.; Oldenbourg, R. Entropy-Driven Formation of a Chiral Liquid-Crystalline Phase of Helical Filaments. *Phys. Rev. Lett.* **2006**, *96*, 018305.
(16) Grelet, E.; Fraden, S. What Is the Origin of Chirality in the Cholesteric Phase of Virus Suspensions? *Phys. Rev. Lett.* **2003**, *90*, 198302.
(17) Mulder, D.-J.; Schenning, A.; Bastiaansen, C. Chiral-Nematic Liquid Crystals as One Dimensional Photonic Materials in Optical Sensors. *J. Mater. Chem. C* **2014**, *2*, 6695−6705.
(18) Knowles, T. P. J.; Buehler, M. J. Nanomechanics of Functional and Pathological Amyloid Materials. *Nat. Nanotechnol.* **2011**, *6*, 469−479.
(19) Knowles, T. P. J.; Mezzenga, R. Amyloid Fibrils as Building Blocks for Natural and Artificial Functional Materials. *Adv. Mater.* **2016**, *28*, 6546−6561.
(20) Nyström, G.; Fernández-Ronco, M. P.; Bolisetty, S.; Mazzotti, M.; Mezzenga, R. Amyloid Templated Gold Aerogels. *Adv. Mater.* **2016**, *28*, 472−478.
(21) Shen, Y.; Posavec, L.; Bolisetty, S.; Hilty, F. M.; Nyström, G.; Kohlbrecher, J.; Hilbe, M.; Rossi, A.; Baumgartner, J.; Zimmermann, M. B.; Mezzenga, R. Amyloid Fibril Systems Reduce, Stabilize and Deliver Bioavailable Nanosized Iron. *Nat. Nanotechnol.* **2017**, *12*, 642−647.
(22) Jung, J. M.; Mezzenga, R. Liquid Crystalline Phase Behavior of Protein Fibers in Water: Experiments *versus* Theory. *Langmuir* **2010**, *26*, 504−514.
(23) Mezzenga, R.; Jung, J. M.; Adamcik, J. Effects of Charge Double Layer and Colloidal Aggregation on the Isotropic-Nematic Transition of Protein Fibers in Water. *Langmuir* **2010**, *26*, 10401−10405.
(24) Sagis, L. M. C.; Veerman, C.; Van Der Linden, E. Mesoscopic Properties of Semiflexible Amyloid Fibrils. *Langmuir* **2004**, *20*, 924−927.
(25) Corrigan, A. M.; Müller, C.; Krebs, M. R. H. The Formation of Nematic Liquid Crystal Phases by Hen Lysozyme Amyloid Fibrils. *J. Am. Chem. Soc.* **2006**, *128*, 14740−14741.
(26) Cherny, I.; Gazit, E. Amyloids: Not Only Pathological Agents but Also Ordered Nanomaterials. *Angew. Chem., Int. Ed.* **2008**, *47*, 4062−4069.
(27) Nyström, G.; Arcari, M.; Mezzenga, R. Confinement-Induced Liquid Crystalline Transitions in Amyloid Fibril Cholesteric Tactoids. *Nat. Nanotechnol.* **2018**, *13*, 330−336.
(28) Adamcik, J.; Jung, J. M.; Flakowski, J.; De Los Rios, P.; Dietler, G.; Mezzenga, R. Understanding Amyloid Aggregation by Statistical Analysis of Atomic Force Microscopy Images. *Nat. Nanotechnol.* **2010**, *5*, 423−428.
(29) Lara, C.; Adamcik, J.; Jordens, S.; Mezzenga, R. General Self-Assembly Mechanism Converting Hydrolyzed Globular Proteins into Giant Multistranded Amyloid Ribbons. *Biomacromolecules* **2011**, *12*, 1868−1875.
(30) Zhao, J.; Bolisetty, S.; Adamcik, J.; Han, J.; Fernández-Ronco, M. P.; Mezzenga, R. Freeze-Thaw Cycling Induced Isotropic-Nematic Coexistence of Amyloid Fibrils Suspensions. *Langmuir* **2016**, *32*, 2492−2499.
(31) Purdy, K. R.; Fraden, S. Isotropic-Cholesteric Phase Transition of Filamentous Virus Suspensions as a Function of Rod Length and Charge. *Phys. Rev. E - Stat. Physics, Plasmas, Fluids, Relat. Interdiscip. Top.* **2004**, *70*, 061703.
(32) Barry, E.; Beller, D.; Dogic, Z. A Model Liquid Crystalline System Based on Rodlike Viruses with Variable Chirality and Persistence Length. *Soft Matter* **2009**, *5*, 2563−2570.
(33) De Michele, C.; Zanchetta, G.; Bellini, T.; Frezza, E.; Ferrarini, A. Hierarchical Propagation of Chirality through Reversible Polymerization: The Cholesteric Phase of DNA Oligomers. *ACS Macro Lett.* **2016**, *5*, 208−212.
(34) Viamontes, J.; Oakes, P. W.; Tang, J. X. Isotropic to Nematic Liquid Crystalline Phase Transition of F -Actin Varies from Continuous to First Order. *Phys. Rev. Lett.* **2006**, *97*, 118103.
(35) Frezza, E.; Tombolato, F.; Ferrarini, A. Right- and Left-Handed Liquid Crystal Assemblies of Oligonucleotides: Phase Chirality as a Reporter of a Change in Non-Chiral Interactions? *Soft Matter* **2011**, *7*, 9291.
(36) Honorato-Rios, C.; Kuhnhold, A.; Bruckner, J. R.; Dannert, R.; Schilling, T.; Lagerwall, J. P. F. Equilibrium Liquid Crystal Phase Diagrams and Detection of Kinetic Arrest in Cellulose Nanocrystal Suspensions. *Front. Mater.* **2016**, *3*, 21.
(37) Onsager, L. The Effects of Shape on the Interaction of Colloidal Particles. *Ann. N. Y. Acad. Sci.* **1949**, *51*, 627−659.
(38) Flory, P. J. Phase Equilibria in Solutions of Rod-Like Particles. *Proc. R. Soc. London, Ser. A* **1956**, *234*, 73−89.
(39) Nyström, G.; Fong, W. K.; Mezzenga, R. Ice-Templated and Cross-Linked Amyloid Fibril Aerogel Scaffolds for Cell Growth. *Biomacromolecules* **2017**, *18*, 2858−2865.
(40) Bouligand, Y.; Livolant, F. The Organization of Cholesteric Spherulites. *J. Phys. (Paris)* **1984**, *45*, 1899−1923.
(41) Prinsen, P.; van der Schoot, P. Shape and Director-Field Transformation of Tactoids. *Phys. Rev. E: Stat. Phys., Plasmas, Fluids, Relat. Interdiscip. Top.* **2003**, *68*, 21701.
(42) Kaznacheev, A. V.; Bogdanov, M. M.; Taraskin, S. A. The Influence of Anchoring Energy on the Prolate Shape of Tactoids in

DOI: 10.1021/acsnano.8b07557
ACS Nano XXXX, XXX, XXX−XXX

Lyotropic Inorganic Liquid Crystals. *J. Exp. Theor. Phys.* **2002**, *95*, 57−63.
(43) Zhou, S. *Lyotropic Chromonic Liquid Crystals*; Springer International Publishing: Cham, 2017.
(44) Odijk, T. Elastic Constants of Nematic Solutions of Rod-like and Semi-Flexible Polymers. *Liq. Cryst.* **1986**, *1*, 553−559.
(45) van der Schoot, P. Remarks on the Interfacial Tension in Colloidal Systems. *J. Phys. Chem. B* **1999**, *103*, 8804−8808.
(46) Jamali, V.; Behabtu, N.; Senyuk, B.; Lee, J. A.; Smalyukh, I. I.; Van Der Schoot, P.; Pasquali, M. Experimental Realization of Crossover in Shape and Director Field of Nematic Tactoids. *Phys. Rev. E - Stat. Nonlinear, Soft Matter Phys.* **2015**, *91*, 042507.
(47) Romani, E.; Ferrarini, A.; De Michele, C. Elastic Constants of Chromonic Liquid Crystals. *Macromolecules* **2018**, *51*, 5409−5419.
(48) Odijk, T. Pitch of a Polymer Cholesteric. *J. Phys. Chem.* **1987**, *91*, 6060−6062.
(49) Odijk, T. Theory of Lyotropic Polymer Liquid Crystals. *Macromolecules* **1986**, *19*, 2313−2329.
(50) Vigolo, D.; Zhao, J.; Handschin, S.; Cao, X.; deMello, A. J.; Mezzenga, R. Continuous Isotropic-Nematic Transition in Amyloid Fibril Suspensions Driven by Thermophoresis. *Sci. Rep.* **2017**, *7*, 1211.
(51) Usov, I.; Mezzenga, R. FiberApp: An Open-Source Software for Tracking and Analyzing Polymers, Filaments, Biomacromolecules, and Fibrous Objects. *Macromolecules* **2015**, *48*, 1269−1280.

DOI: 10.1021/acsnano.8b07557
ACS Nano XXXX, XXX, XXX−XXX